Global Maximum Power Point Tracking of Flexible Photovoltaic Modules

Christos Konstantopoulos and Eftichios Koutroulis, *Member, IEEE*

***Abstract*—The flexible photovoltaic (PV) modules have the advantage of easily fitting on curved surfaces, but in that case their power–voltage characteristic exhibits local maximum power points (MPPs) where the PV module power production is suboptimal. In this paper, the effect of geometrical installation parameters of flexible PV modules, such as the bending angle, tilt angle, and orientation, on the shape of the power–voltage characteristic is experimentally investigated. Then, a new method of tracking the global MPP of flexible PV modules is proposed. An experimental, comparative study is also presented, which demonstrates that compared to the past-proposed MPP tracking (MPPT) techniques, the system proposed in this paper is capable to detect the global MPP of a flexible PV module with less search steps. Thus, the power loss during the global MPPT process is minimized and the energy production of the flexible PV module is maximized.**

***Index Terms*—Flexible, maximum power point tracking (MPPT), microcontroller, photovoltaic (PV) module.**

I. Introduction

THE use of flexible photovoltaic (PV) modules has emerged during the past few years for solar energy production on portable, wearable, and mobile electronic devices, as well as aerospace and building-integrated PV (BIPV) systems [1]–[4]. Flexible PV modules have the capability to fit on nonplanar surfaces, thus easily adapting to the architectural topology of the installation structure (e.g., roof tiles, facades, tents, etc.). They are fabricated using multiple, series-connected thin solar cells (e.g., using monocrystalline or amorphous silicon, Copper Indium Gallium Selenide (CIGS) semiconductor, etc., of 2–100 μm typical thickness), which are encapsulated within a flexible material (e.g., silicone gel) [5]–[7]. They are capable to operate without loss of performance when installed on curved surfaces [2] with a typical efficiency in the range of 13%–23%, depending on their manufacturing technology [2], [3], [5], [7]. Also, due to their rollable/foldable features, flexible PV modules enable easy transport and storage [5].

Typically, the commercially available flat-plate PV modules consist of multiple solar cells connected in series. A bypass diode is connected in parallel to each module (or group of cells within a module) for protection against hot-spot failure effects. As illustrated in Fig. 1, under no-partial-shading conditions, the power–voltage characteristic of the individual PV modules exhibits a unique maximum power point (MPP) [8], [9]. The position and magnitude of the MPP depends on the solar irradiation and ambient temperature operating conditions. By controlling a power electronic converter, which is connected at the output of the PV module or array, according to an MPP tracking (MPPT) technique [10]–[12], the PV power-generator always operates at the corresponding MPP under the continuously variable meteorological conditions and the PV energy production is maximized. Extensive reviews of the techniques, which have been proposed to perform the MPPT process for PV modules operating under such uniform solar irradiation conditions, as well as their operational characteristics, are included in [13]–[15].

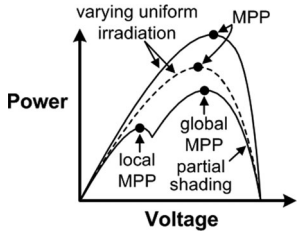

Fig. 1. Power–voltage characteristic of flat-plate PV modules and arrays under uniform and partial-shading conditions.

For PV arrays formed by flat-plate PV modules, in case that the individual PV modules comprising the PV array receive unequal amounts of solar irradiation (e.g., due to dust, shading from surrounding buildings, etc.) then the power–voltage characteristic of the PV array exhibits multiple local maxima and only one of them corresponds to the global MPP (see Fig. 1). In [16], it is shown that local maxima of small amplitude, called "traps", could also be observed in a measured PV power curve due to circuit nonidealities causing measurement errors with amplitude which is a function of the PV voltage. A generalized perturb and observe (P&O) MPPT algorithm is proposed in [16] in order to avoid convergence of the tracking algorithm to the local MPPs on such "traps". However, the performance of this algorithm under the existence of large-amplitude local MPPs, such as those encountered under partial shading conditions, has not been investigated.

The installation of a separate dc/dc converter with MPPT capability at each PV module or group of solar cells within the module, thus forming a distributed MPPT system, has been described in [17]–[19] in order to avoid the impact of partial shading of the individual PV modules and maximize the energy production of the entire PV array. In [20], multiple power

Manuscript received March 28, 2013; revised June 20, 2013; accepted July 22, 2013. Date of current version January 29, 2014. Recommended for publication by Associate Editor C. A. Canesin.

The authors are with the Department of Electronic and Computer Engineering, Technical University of Crete, Chania GR-73100, Greece (e-mail: ckons89@gmail.com; efkout@electronics.tuc.gr).

Color versions of one or more of the figures in this paper are available online at http://ieeexplore.ieee.org.

Digital Object Identifier 10.1109/TPEL.2013.2275947

0885-8993 © 2013 IEEE. Personal use is permitted, but republication/redistribution requires IEEE permission.
See http://www.ieee.org/publications_standards/publications/rights/index.html for more information.

switches, diodes, and capacitors are distributed among groups of series-connected solar cells within a PV module. In that scheme, the power switches are controlled such that in case of nonuniform solar irradiation incidence among the individual groups of solar cells, each of them still operates at its local MPP by redistributing the produced energy between the groups of solar cells through the use of an inductor. A similar topology is proposed in [21] in order to maximize the energy production of PV sources which are connected in series at the input of a multilevel dc-link inverter under partial shading conditions. In flat-plate PV module configurations, the power–voltage curve of the PV array may exhibit multiple local MPPs in case that multiple PV elements (cells or modules) are connected in series and the incident solar irradiation is nonuniform among them (see Fig. 1). However, as will be demonstrated in the following sections of this paper, this effect also arises for the individual flexible PV modules, even in case that they are not connected in series or parallel with other PV modules. Thus, the installation of a separate dc/dc converter at each flexible PV module is not adequate to guarantee that the maximum PV module power is produced, unless a suitable global MPPT method is applied.

In [22], the position of the global MPP of a PV array operating under partial shading conditions is detected by changing a voltage reference proportionally to the ratio of the PV array open-circuit voltage and short-circuit current. The application of this method requires knowledge of the configuration of the PV modules within the PV array (i.e., number of PV modules connected in series and parallel) and their operational characteristics.

In [23], the global MPP is detected by iteratively modifying (with a fixed step) the duty cycle of a dc/dc power converter, which is connected at the output of the PV array, such that the entire power–voltage curve of the PV array is scanned. The same principle is also applied in [24], where a switched-capacitor dc/dc converter is used for continuously tracking the MPP of a partially shaded PV array. The global MPP detection process is performed by periodically scanning the power–voltage curve of the PV array using a MOSFET power switch connected in parallel to the PV array, which is controlled a such that it is driven from cutoff to saturation through the active region. Thus, the entire power–voltage characteristic of the PV array, from the open-circuit voltage to the short-circuit current operating points, is scanned in order to derive the position of the global MPP.

A review of past-proposed techniques for the appropriate configuration of the electrical connections among the PV modules comprising the PV array or their dynamic reconfiguration using a matrix of power switches, in order to minimize the power loss due to partial shading, is presented in [25]. However, these methods are not adequate to ensure maximum power production under all partial shading conditions. Furthermore, in case of the dynamic reconfiguration strategy, the switch matrix and associated wiring for performing the interconnections between the PV cells/modules result in increased hardware complexity [26].

The application of a radial basis function and a three layered feed-forward neural network is proposed in [27] for tracking the global MPP. Using such an approach has the disadvantage that the hardware resources required for implementing the control unit are increased. Also, intensive efforts are required by the system designer in order to ensure that the neural network training process will be adequate to ensure convergence to the global MPP under any partial shading conditions. The global MPPT scheme based on the DIviding RECTangles (DIRECT) optimization algorithm, which is presented in [28], does not guarantee that the global MPP detection process can be accomplished in fewer steps than those required for sequentially scanning the power–voltage characteristic of the PV array.

A chaotic-search process based on two recursive functions (i.e., dual carrier), which produce possible positions of the global MPP in the search space, is presented in [29] in order to track the global MPP under partial shading conditions and simultaneously improve the efficiency of the conventional chaos-theory-based search algorithm. In that work, a heuristic algorithm is proposed that performs iterative fragmentations of the PV array power–voltage characteristic, utilizing sequences of numbers, which are generated through the use of appropriate functions and correspond to alternative operating points on the power–voltage characteristic of the PV array. The global optimum is detected by measuring and comparing the power generated by the PV array at these positions.

The deployment of evolutionary algorithms (EAs) has been proposed in order to detect the global MPP of partially shaded PV arrays, due to their ability to overcome the multiple local MPPs barrier and detect the global optimum MPP. Among the EAs, the particle swarm optimization (PSO) and differential evolution (DE) algorithms have been proposed in [30]–[32], respectively, due to their implementation simplicity and robustness features.

In the standard PSO method, a swarm of particles moves in a search space with dimension equal to the number of decision variables of the optimization problem, by cooperating among them while searching for the global optimum point [31]. The next movement of each particle within the search space is influenced by its local best known position in combination with the best known position among the entire set of particles. The use of deterministic PSO has been proposed in [33] to improve the tracking capability of the conventional PSO algorithm, mainly by removing the randomness from the calculation of the PSO particles velocity.

The DE algorithm is a stochastic, population-based optimization algorithm. The optimization process is conducted similarly to genetic algorithms using the crossover, mutation, and selection operators [32]. The main difference with genetic algorithms is that the latter relies on crossover, while DE uses the mutation operation as a search mechanism and the selection operation to direct the members of the population within the search space toward the regions where the fitness (i.e., objective) function is maximized.

In commercially available flexible PV modules, bypass diodes are connected in parallel with the individual cells comprising the PV module. Targeting to a higher degree of integration in distributed MPPT applications, the incorporation of the dc/dc converter into the structure of a flexible PV module using the back layer of the PV module as a substrate instead of a PCB, is described in [34]. However, in case that a flexible PV module

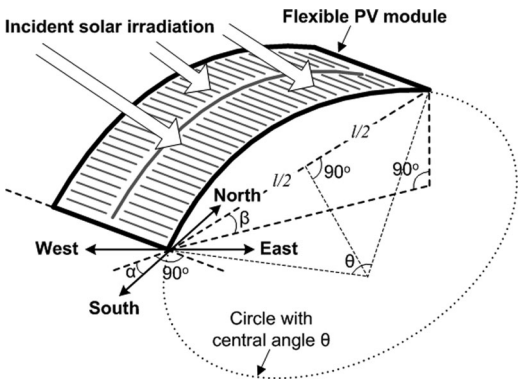

Fig. 2. Geometrical model of a flexible PV module under bending conditions.

is installed on a bended surface then different solar irradiation intensity is incident on each of the solar cells it comprises. Thus, as will be demonstrated next, its power–voltage characteristic may exhibit local maxima (as those depicted in Fig. 1), although the flexible PV module operates under no partial-shading conditions. The MPPT method applied in [35] for flexible PV modules is characterized by increased implementation complexity, since knowledge of the incident solar irradiance, as well as the contour angle and open-circuit voltage of the flexible PV module are required for the detection of the global MPP. Until present, the issue of MPPT of flexible PV modules has not been studied any further.

In this paper, the operational characteristics of flexible PV modules are initially investigated in order to explore the impact of solar irradiation conditions and installation geometry on the current–voltage and power–voltage characteristics of flexible PV modules and derive the corresponding operational requirements of a global MPPT algorithm, which is suitable for applications of flexible PV modules. This issue is explored in this paper for the first time in the existing research literature. Then, a new method for tracking the global MPP of flexible PV modules is proposed, which, compared to the past-proposed global MPPT techniques, has the advantage of being able to detect the global MPP in less search steps, thus minimizing the power loss during the global MPPT process. The proposed method is suitable for incorporation in commercial PV power processing products, since it does not require knowledge of the operational characteristics of the flexible PV modules comprising the installed PV system. Such information is typically available during the PV system design process, which is performed after the MPPT device has been manufactured.

This paper is organized as follows: the operational characteristics of flexible PV modules are presented in Section II; the proposed global MPPT system is analyzed in Section III; finally, the experimental results are presented in Section IV.

II. Operational Characteristics of Flexible PV Modules

The general installation geometry of a flexible PV module under bending conditions is shown in Fig. 2. The PV module slope is defined by the angle $\beta(^\circ)$ between the horizontal plane and the chord of the arc formed by the bended PV module. Additionally, the PV module is installed with an azimuth angle equal to $\alpha(^\circ)$ with respect to the north–south axis. A different amount of solar irradiation is incident on each point of the flexible PV module, since the angle of incidence of the solar irradiation varies continuously along the PV module surface. Under bending conditions, the flexible PV module forms an arc in a circle. The degree of bending of the flexible PV module is expressed by the central angle θ (in degrees, $0^\circ \leq \theta \leq 180^\circ$), having its vertex at the center of that circle and its sides passing through the edges of the flexible PV module. Applying geometrical calculations results that the length l (in meters) of the chord which is formed between the two edges of the bended PV module (see Fig. 2) is given by

$$l = \begin{cases} 2L\sin(\theta/2)\dfrac{180^\circ}{\pi\cdot\theta}, & \text{for } 0^\circ < \theta \leq 180^\circ \\ L, & \text{for } \theta = 0^\circ \end{cases} \quad (1)$$

where L (in meters) is the length of the arc formed by the flexible PV module, which is also equal to the length of the PV module.

Until present, there is no suitable mathematical model available in the existing research literature for calculating the output current and power of a flexible PV module as a function of the bending, azimuth and slope installation settings. Thus, in order to explore the behavior of a flexible PV module under various installation conditions in this paper, its current–voltage and power–voltage characteristics were experimentally measured using a suitable data-acquisition system, for various values of θ, β, and α during consecutive clear-sky summer days.

The current–voltage and power–voltage characteristics of a south-facing flexible PV module (i.e., $\alpha = 0^\circ$ in Fig. 2) with $\beta = 0^\circ$ for various bending angles in the range $\theta = 0^\circ$–180° are illustrated in Fig. 3. The current–voltage and power–voltage characteristics of the same flexible PV module with $\beta = 45^\circ$ at 12:00 of consecutive clear-sky summer days for various values of θ and α are depicted in Fig. 4. The corresponding solar irradiation and ambient temperature conditions are also indicated in both of these figures. It is observed that the installation geometry relatively to the direction of sun rays, in terms of θ, α, and β, affects the shape of the current–voltage and power–voltage characteristics. Compared to the case that $\theta = 0^\circ$, increasing the degree of bending of the flexible PV module (i.e., parameter θ) results in the development of local MPPs and/or regions where the power gradient tends to zero. The number of local MPPs varies from one hour to another, depending on the extent of the nonuniform solar irradiation incidence across the PV module surface as time (i.e., solar angle) changes during the day. Both Figs. 3 and 4 reveal that the position of the global MPP is not fixed, but changes according to time, installation geometry of the flexible PV module in terms of θ, α, and β, as well as the prevailing solar irradiation and ambient temperature conditions, which result in different incident solar irradiation conditions among the individual solar cells comprising the flexible PV module. Thus, the development of a suitable MPPT system is required, which is capable to detect the global MPP of the flexible PV module under any installation geometry and meteorological operating conditions.

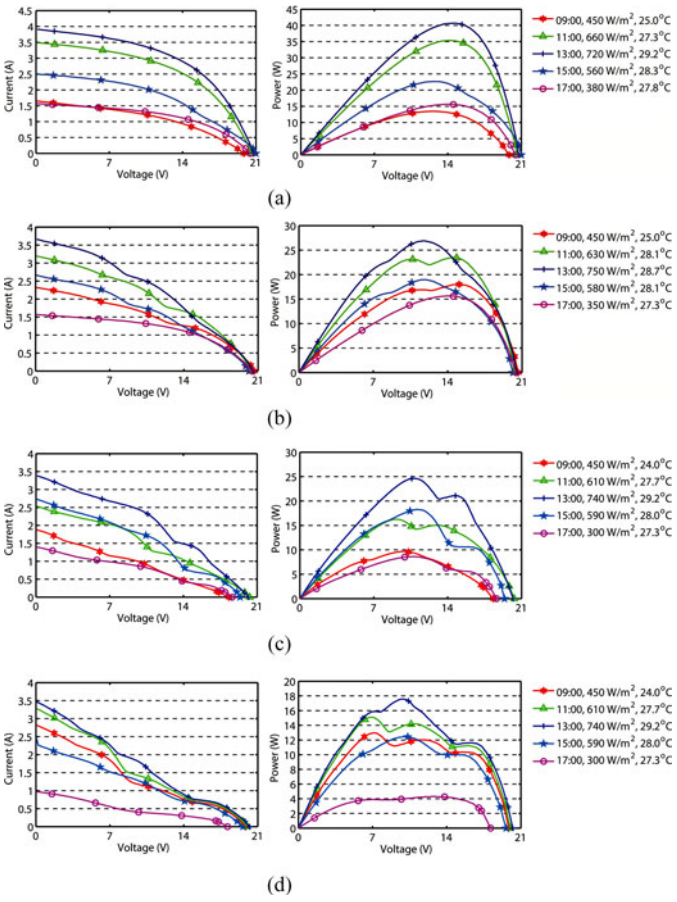

Fig. 3. Current–voltage and power–voltage characteristics of a south-facing flexible PV module ($\alpha = 0°$) with $\beta = 0°$ under various bending conditions during clear-sky summer days: (a) $\theta = 0°$; (b) $\theta = 60°$; (c) $\theta = 120°$; and (d) $\theta = 180°$.

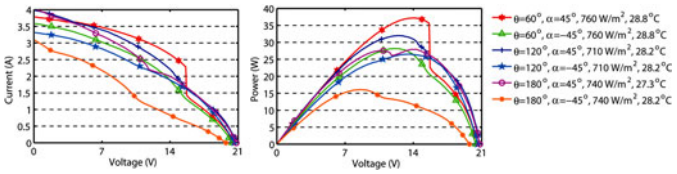

Fig. 4. Current–voltage and power–voltage characteristics of a flexible PV module with $\beta = 45°$ at 12:00 of consecutive clear-sky summer days, for various values of θ and α.

III. Proposed Global MPPT System for Flexible PV Modules

A block diagram of the proposed global MPPT system for flexible PV modules is illustrated in Fig. 5. A boost-type dc/dc converter is used in order to interface the power generated by the flexible PV module to a voltage source (either a battery bank or a grid-connected dc/ac inverter). The flexible PV module operates under bending conditions, as analyzed in Section II. An RS-232 communication interface has been employed for transferring the measurements acquired by the microcontroller to a computer, in order to analyze the performance of the proposed system. The value of the input inductor $L_{\rm in}$ (in henry) is calculated such that the dc/dc converter operates in the continuous conduction mode.

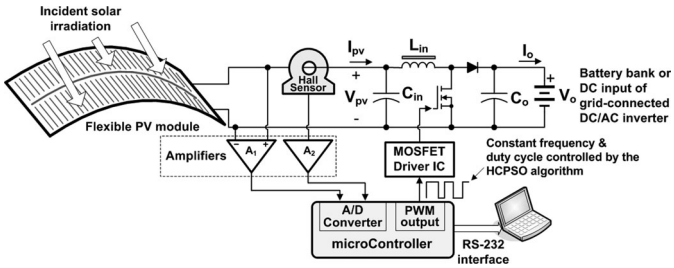

Fig. 5. Block diagram of the proposed global MPPT system for flexible PV modules.

In this operating mode, the input/output voltage relationship is given by [36]

$$\frac{V_o}{V_{pv}} = \frac{1}{1-D} \tag{2}$$

where V_{pv} and V_o (in volts) are the input and output voltage, respectively, of the dc/dc converter and D is the duty cycle of the pulsewidth modulated (PWM) signal $(0 \leq D < 1)$, which controls the power MOSFET of the dc/dc converter according to the proposed global MPPT algorithm analyzed in the following.

The maximum permissible value of D in (2) depends on the specifications of the dc/dc converter operating input- and output-voltage ranges, the period of the PWM control signal, as well as the turn-on and turn-off delay times of the power semiconductor devices employed in the dc/dc converter. The values of the input and output capacitors $C_{\rm in}$ and C_o (in farad) are calculated as analyzed in [36] and [37], such that the peak-to-peak ripples of the PV module output current and dc/dc converter output voltage, respectively, are constrained to be less than the maximum permitted limits. A microcontroller unit executes the global MPPT algorithm, using the measurements of the PV module output voltage and current V_{pv} and I_{pv} in Fig. 5, respectively, which are acquired by an analog-to-digital converter (A/D), as analyzed next.

As demonstrated in Section II, local maxima appear on the power–voltage characteristic of flexible PV modules under bending conditions. During the execution of a global MPP search process, the PV module is iteratively set to operate at various nonoptimal power/voltage operating points. Thus, in order to minimize the power loss during the search process it is required to apply an efficient algorithm, which is capable to track the global MPP with the minimum possible number of search steps. In case of convergence to a local optimum, the conventional PSO algorithm performs a random reinitialization of the particles positions, which results in scattering the swarm over the entire power–voltage characteristic [31]. However, this process is not always effective, since the time required for convergence to the global MPP is increased. During the execution of the chaotic-search algorithm, sequences of unequal numbers (chaotic sequences) are iteratively produced during successive time steps according to special deterministic functions (chaotic maps) [29], which results in a scattered search as dictated by the chaotic maps. In contrast to these approaches, in this paper it is proposed to perform the global MPPT process using a combination of the dual-carrier (i.e., using two recursive functions)

chaotic-search and PSO optimization algorithms, comprising the hybrid chaotic-PSO algorithm (HCPSO). As will be analyzed next, the proposed HCPSO algorithm features a local and a scattered search process by detecting positions that are better than the current best position of each particle, in terms of the PV module power generation, without taking into account the best positions discovered by the other particles of the population. It is based on the PSO convergence mechanism, utilizing the cooperative intelligence of particles in order to avoid the computational complexity of the corresponding operation of the chaotic-search process, but also whenever the particles converge and stall to local MPPs the HCPSO algorithm uses chaotic sequences in order to reinitialize the particles and escape from these points in order to continue searching for the global MPP. The integration of a chaotic-search process into the PSO algorithm has also been proposed in [38], which is not relevant to power maximization in PV systems. However, the HCPSO algorithm presented in this paper performs the optimization procedure based on two chaotic maps, instead of the single chaotic map applied in [38]. Furthermore, a more efficient termination condition is applied in the proposed HCPSO algorithm, which is based on the evolution of an utmost number of chaotic generations that in worst case are permitted to elapse during the exploration of the search space, when the search procedure is not able to derive a better solution than the current personal best position of each particle. These two operational characteristics aim to increase the speed of convergence to the global MPP.

In the proposed HCPSO algorithm, the chaotic-search process for the ith particle is performed using the following recursive chaotic maps [29]:

$$y_t = 4 \cdot y_{t-1} \cdot (1 - y_{t-1}) \tag{3}$$

$$x_t = 2 \cdot x_{t-1} \cdot \sin(\pi \cdot x_{t-1}) \tag{4}$$

where $[x_{t-1}, y_{t-1}]$ and $[x_t, y_t]$ are the logistic and sine chaotic variables, respectively, at search steps $t-1$ and t, respectively.

The logistic chaotic mapping in (3) enables to execute a scattered search at distant positions around the current position, while the sine chaotic map in (4) offers a local search capability.

A flowchart of the proposed HCPSO algorithm is depicted in Fig. 6. An initial population of N particles is initially created. According to the PSO mechanism which is embedded in the HCPSO algorithm, the ith particle has a position (i.e., a value of the PV module voltage on the power–voltage characteristic of the flexible PV module) represented by a position vector x_i and a velocity represented by the velocity vector v_i [31]. Each particle stores its own best position discovered so far in parameter $p\text{Best}_i$. The best position detected by the entire swarm until the current search step is the parameter pGlobal, and its value (i.e., the corresponding output power of the flexible PV module) is the parameter gBest. The velocity of the ith particle at the current search step t is updated using the corresponding value at step $t-1$, as follows [31]:

$$v_i(t) = x \cdot [w \cdot v_i(t-1) + c_1 \cdot r_1 \cdot p\text{Best}_i(t-1) - c_1 \cdot r_1 \cdot s_i(t-1) + c_2 \cdot r_2 \cdot g\text{Best}(t-1) - c_2 \cdot r_2 \cdot s_i(t-1)] \tag{5}$$

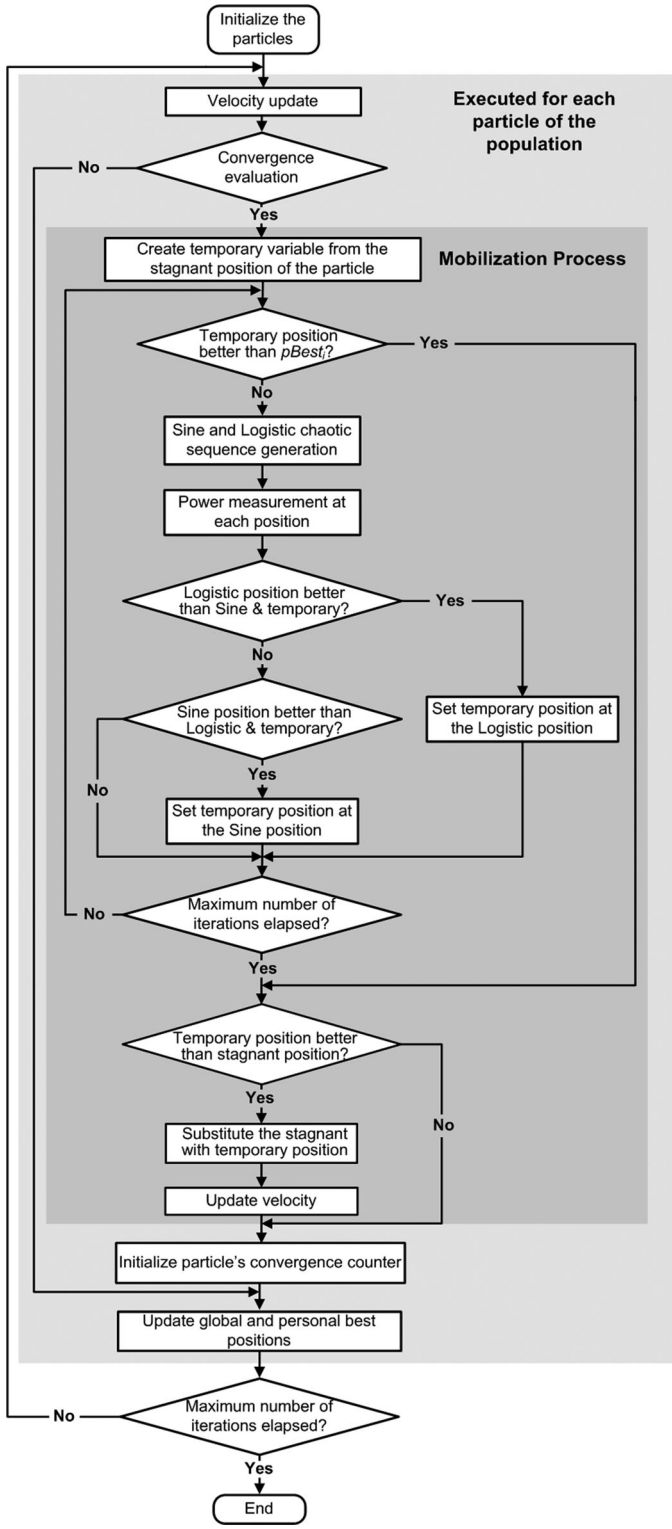

Fig. 6. Flowchart of the proposed HCPSO algorithm.

where r_1 and r_2 are random numbers uniformly distributed within the interval [0, 1], c_1 is the positive self-recognition coefficient, c_2 is the social coefficient, w is the momentum factor, and x is the constriction factor.

At each position, the PV module output power is calculated as the product of the PV module output voltage and current

V_{pv} and I_{pv}, respectively, which are measured through the A/D converter (see Fig. 5).

Each particle decides about the direction toward to move next, considering its own experience (i.e., its own best past position) and the experience of the most successful particle in the swarm. Thus, the position of the ith particle at search step t $s_i(t)$ is calculated as the sum of its position at time step $t-1$ and the new velocity $v_i(t)$

$$s_i(t) = s_i(t-1) + v_i(t). \tag{6}$$

The positions of the particles correspond to 8-bit integer values of the dc/dc converter duty cycle, D in (2) (i.e., 128-255), according to the following equation:

$$D = \text{floor}\,[s_i(t)] \tag{7}$$

where the floor$(\cdot)$ function rounds down the calculated position value.

In contrast to the approach applied in the PSO method, the values of the initial set of particles in the proposed HCPSO algorithm are assigned based on the logistic chaotic variables according to the following equation:

$$s_i(t=0) = b + (a-b)\cdot y_i \tag{8}$$

where $s_i(t=0)$ is the initial position of the ith particle $(1 \le i \le N)$, and $a = 255$ and $b = 128$ are the maximum and minimum values, respectively, of the possible positions range (i.e., 8-bit integer values of the dc/dc converter duty cycle in the range of 128–255) and y_i is given by (3) by setting $t = i$.

The HCPSO algorithm considers that a particle is stagnant, thus not been able to discover better positions, whenever both of the following conditions apply for two consecutive time steps:

$$|v_i(t)| < \Delta s \tag{9}$$

$$\left|\frac{P(s_i(t)) - P(p\text{Best}_i(t))}{P(s_i(t))}\right| < \Delta P \tag{10}$$

where $P(s_i(t))$ and $P(p\text{Best}_i(t))$ (in watts) are the PV power produced by the ith particle at positions $s_i(t)$ and $p\text{Best}_i(t)$, respectively, and Δs and ΔP are the voltage and power stagnancy limits, respectively, and their values are set by the MPPT system designer.

In order to overcome the particle's stagnancy condition and retrigger the search process of the stagnant particle to explore the position of the global MPP, the chaotic-search-based mobilization process illustrated in Fig. 6 is then executed for the stagnant particle. The local position of the stagnant particle is assigned to a temporary variable. Then, a close and a distant operating point of the flexible PV module (i.e., positions on the power–voltage characteristic) are generated according to the chaotic maps, with respect to the local position of the particle, which both explore for possible better positions in terms of the PV-generated power. In order to check whether there is any other distant area with a batch of better positions than the currently focused area, the distant and close positions are compared with the temporary position in terms of the power generated by the flexible PV module at each of these points. Then, the power generated by the flexible PV module is measured at positions $y\text{Log}_t$ and $x\text{Sin}_t$, which correspond to the distant and close positions, respectively. These positions are generated by utilizing the chaotic variables y_t and x_t at search step t, which are given by the recursive chaotic maps in (3) and (4), respectively, as follows:

$$y\text{Log}_t = s_{\text{temp}} + (a-b)\cdot(k\cdot y_t - 0.5)/\text{div}_{\text{Log}} \tag{11}$$

$$x\text{Sin}_t = s_{\text{temp}} + (a-b)\cdot(g\cdot x_t - 1.2)/\text{div}_{\text{Sin}} \tag{12}$$

where s_{temp} is the temporary position, while $k, g, \text{div}_{\text{Sin}}, \text{div}_{\text{Log}}$ are scaling parameters and their values are determined empirically.

Initially (i.e., for $t = 0$), the values of the chaotic variables y_t and x_t are set equal to 0.6 and 0.9, respectively. The power generated at $y\text{Log}_t, x\text{Sin}_t$, as well as at the temporal position, are compared according to the following steps:

1) If the power generated at the position $y\text{Log}_t$ is higher than the power produced at the temporary position and the power generated at $x\text{Sin}_t$, then the temporary position is substituted by $y\text{Log}_t$.
2) If the power generated at $x\text{Sin}_t$ is higher than the power produced at the temporary position and the power generated at $y\text{Log}_t$, then the temporary position is substituted by $x\text{Sin}_t$.
3) If the power generated at the temporary position resulting after steps 1) and 2) is less than or equal to the power at $p\text{Best}_i$, then the chaotic search procedure is repeated by producing new logistic and sine chaotic variables using the temporary position of time step $t-1$.
4) If the power generated at the temporary position which results after steps 1) and 2) is higher than $p\text{Best}_i$, or a maximum permitted number of iterations G_2 has elapsed, then the chaotic-search operation is suspended.

In case that after step 4) the mobilization process has discovered a temporary position which is better than the particle's stagnant position before the mobilization process, then the stagnant position is substituted with the position indicated by the temporary position and the velocity of the particle is updated as follows:

$$v_i(t) = s_{\text{temp}} - s_i(t) \tag{13}$$

where s_{temp} is the temporary position.

The mobilization process described earlier performs two changes of the power converter duty cycle within each iteration. When the execution of the mobilization process has been accomplished, then the variable that stores the number of successive generations that the specific particle is stagnant is reset to zero.

At the last step of the HCPSO global MPPT algorithm, the global as well as the personal best position of each particle of the population are updated as follows:

1) If $P(s_i(t)) > P(p\text{Best})$, then $p\text{Best} = s_i(t)$.
2) If $P(s_i(t)) > P(g\text{Best})$, then $g\text{Best} = s_i(t)$.

The HCPSO algorithm described earlier is executed for each particle of the population and is repeated until a predefined number of population generations G_1 have evolved. The operating point where the overall maximum power has been discovered to

Fig. 7. Flexible PV module experimental setup for the performance evaluation of the proposed global MPPT system (in this example the bending angle is $\theta = 90^{\circ}$).

be produced by the flexible PV module is stored in pGlobal and gBest, respectively, as described earlier, and it is considered to be the global MPP of the PV power maximization procedure.

The position of the global MPP of the flexible PV module is derived by executing periodically the proposed HCPSO algorithm, with a repetition period of a few minutes. Then, a conventional MPPT algorithm [15] may be executed in order to continuously track the short-term changes of the previously detected global MPP.

IV. Experimental Results

A laboratory prototype of the proposed system (see Fig. 5) has been designed and constructed in order to evaluate the performance of the proposed global MPPT method experimentally. A dc/dc boost converter is used to interface into a 48 V battery bank the power produced by a UniSolar PVL-68 amorphous-silicon flexible PV module with 68 W/16.5 V MPP power and voltage levels under standard test conditions (STC). Bypass diodes are connected in antiparallel with the solar cells comprising the flexible PV module. The dc/dc boost converter consists of an IRFZ44 power MOSFET and an MBR1060 diode, which operate with a 39 kHz switching frequency. An $L_{\rm in} = 160$ μH input inductance is used for continuous conduction of the dc/dc converter down to an 1 A of dc input current, while the output capacitance C_o has been set to 330 μF in order to achieve a 2% output voltage ripple. The Atmel ATmega 8535 microcontroller unit, embedded in the STK500 development board, is used to execute the MPPT algorithm and produce an 8-bit PWM signal with the appropriate duty cycle, according to the HCPSO algorithm described in Section III. The generated PWM control signal is then interfaced to the boost-type dc/dc power converter through an ICL7667 MOSFET driver IC. The PV module output current is measured using the LTSR6-NP Hall-effect-type current sensor with three turns. As illustrated in Fig. 5, the output of the Hall-effect sensor is interfaced to the A/D converter, which is available on the ATmega 8535 microcontroller chip, through an operational-amplifier-based (LM358) amplifier. The PV module output voltage is measured using a differential amplifier based on the LM358 operational amplifier. The experimental setup which was used to evaluate the performance of the proposed global MPPT system is illustrated in Fig. 7. A suitable supporting frame was constructed, enabling the adjustment of the angles of bending, tilt and orientation of the flexible PV module during the test process, to the desired values.

TABLE I
Operational Parameters of the HCPSO Algorithm

w	c_1	c_2	Δs	ΔP	x	G_1	div_{Log}	div_{Sin}	k	g	G_2	α	b
0.8	1.1	1.3	3	0.05	0.8	10	3	4	1.29	1.1	3	255	128

The experimental setup described earlier was used to evaluate the performance of the dual-carrier chaotic-search [29], PSO [31], DE [32], and HCPSO global MPPT algorithms under real (i.e., outdoors) conditions. The maximum permitted number of generations that each MPPT algorithm is executed was set according to simulation and experimental tests, such that convergence is ensured with the minimum number of search steps in case that the PV module is installed at a horizontal position (i.e., $\theta = 0^{\circ}$). However, since the PSO, DE and HCPSO algorithms execute random procedures in order to initialize and/or direct the particles during the optimization process, the actual number of steps required for their convergence is not constant and these algorithms were executed several times in order to derive the most suitable number of generations. Thus, the PSO and DE algorithms were set to operate for 15 and 10 generations, respectively. The values of the rest of the parameters of the chaotic-search, PSO, and DE algorithms were selected as described in [29], [31] and [32], respectively. For comparison purposes, the proposed HCPSO global MPPT algorithm was set to utilize the same basic parameters as the PSO algorithm, while the rest of the HCPSO algorithm parameters were selected experimentally such that convergence is achieved with the minimum number of steps when $\theta = 0^{\circ}$. The operational parameters of the proposed HCPSO algorithm are shown in Table I. The maximum number of search iterations in case of particle stagnancy were set equal to $G_2 = 3$, as a tradeoff between the improvement capability of the particles to discover better personal positions and the additional search steps that the chaotic-search mobilization procedure imposes (see Fig. 6), which increase the time until convergence to the global MPP has been achieved. The process described earlier for the detection of the MPPT algorithms operational-parameters values, was applied only once, before the initiation of normal operation of the global MPPT system, where the flexible PV module was set to operate under various solar irradiation and bending conditions, as analyzed in the following.

In order to evaluate the convergence speed of the global MPPT algorithms under study, the total number of search steps has been used as a metric, instead of the total convergence time, since it is independent of design- and application-specific parameters, such as the type of the controller (e.g., proportional–integral (PI), proportional-integral-derivative (PID), fuzzy, etc.), the dc/dc converter power rating and input/output voltage specifications, etc. The accuracy of convergence was evaluated by calculating the deviation of the PV-generated power at the final operating point, which has been derived as the global MPP by each MPPT algorithm, from the power production at the actual global MPP of the flexible PV module, which was

detected by applying, prior to the execution of each MPPT algorithm, an exhaustive-search process with the maximum possible resolution of the PWM control signal duty cycle. During the exhaustive-search process, the entire power–voltage characteristic of the flexible PV module was scanned by iteratively modifying the duty cycle of the boost-type dc/dc converter control signal and measuring the power generated by the PV module at the resulting operating points. Since an 8-bit PWM signal is used to control the dc/dc power converter, then for the PV module/battery voltage ranges applied in this experimental setup, the power–voltage characteristic of the flexible PV module was measured in 128 consecutive search steps by the exhaustive-search algorithm in order to detect the global MPP. The power deviation of the final operating point derived by each MPPT algorithm as the global MPP, from the global MPP detected by the exhaustive-search process depends on the operational efficiency of each optimization method, the power measurement errors and the small-scale variations of the solar irradiation and ambient temperature conditions during the exhaustive-search and global MPPT processes, which slightly modify the power–voltage characteristic of the flexible PV module.

A critical parameter determining the performance of the PSO, chaotic-search, DE, and HCPSO global MPPT algorithms is the number of particles/genes comprising each generation. In order to investigate the effect of this parameter, the performance of the PSO, chaotic-search, DE, and HCPSO global MPPT methods under study was initially evaluated in case that the flexible PV module is installed with $\theta = 0^\circ$, such that its power–voltage characteristic exhibits a unique MPP, without additional local MPPs. The DE algorithm was tested for cases that it comprises more than four genes, since for lower values it was not able to successfully detect the global MPP of the flexible PV module. The HCPSO, PSO, and DE algorithms successfully derived the global MPP, which has been measured using an exhaustive-search method as analyzed earlier, with a deviation of less than 1.3%, except of the case of the DE algorithm with five genes where the deviation was increased to 17.7%. The chaotic-search algorithm was also executed for four particles, similarly to the proposed HCPSO algorithm, but it converged to a suboptimal operating point. It was experimentally verified that in order to be capable to track the global MPP successfully, more than eight particles should be included in the chaotic-search algorithm, but this results in higher computational complexity compared to the proposed HCPSO algorithm incorporating two to four particles, due to the sorting process employed. Thus, the performance of the chaotic-search technique was not explored any further.

The experimentally measured numbers of steps required for convergence to the global MPP by each algorithm in case that $\theta = 0^\circ$, for various numbers of particles/genes in each generation of the corresponding populations, are presented in Table II. The number of steps required by the DE method is significantly higher, since two search steps are executed for every gene of DE within the same generation, thus the operation of this algorithm using a higher number of genes within each generation, beyond the configurations illustrated in Table II, was not further investigated. The number of search steps required by the proposed HCPSO algorithm are 6.7%–33.3% and 35.7%–84.1% less than the corresponding numbers of steps required by the PSO (when configured with equal numbers of particles with the HCPSO process) and DE algorithms, respectively.

TABLE II
PERFORMANCE OF THE HCPSO, PSO, AND DE ALGORITHMS FOR VARIOUS VALUES OF θ AND NUMBERS OF PARTICLES/GENES AT 13:00 OF A CLEAR-SKY WINTER DAY

	$\theta = 0^o$	$\theta = 60^o$	$\theta = 120^o$	$\theta = 180^o$
HCPSO				
Number of particles	**Number of steps**			
2	20	30	20	20
3	42	38	36	48
4	54	40	42	40
PSO				
Number of particles	**Number of steps**			
2	30	30	30	30
3	45	45	45	45
4	60	60	60	60
DE				
Number of genes	**Number of steps**			
4	84	84	84	84
5	105	105	105	105
6	126	126	126	126

Then, the bending angle of the flexible PV module was increased to $\theta = 60^\circ, 120^\circ$, and 180°, respectively and the previous test process was repeated. By measuring the power–voltage characteristic of the flexible PV module it was detected that for the specific meteorological and installation conditions of this test process, it exhibits a unique MPP for $\theta = 60^\circ$ and 120°, while an additional local MPP is contained for $\theta = 180^\circ$. The corresponding experimental results are summarized in Table II. The PSO algorithm is faster than the proposed HCPSO process by 6.3% only in case that they both employ three particles in order to perform the MPPT process. In the rest of the cases investigated, the number of search steps required by the proposed HCPSO algorithm are less than the search steps required by the PSO (for the configurations with equal numbers of particles with the HCPSO process) and DE algorithms by 0%–33.3% and 42.9%–84.1%, respectively. In contrast to the PSO- and DE-based global MPPT methods, the number of search steps executed in the proposed HCPSO algorithm is not constant due to the activation of the chaotic-search-based mobilization mechanism for the particles under stagnancy (see Fig. 6). The average value of the relative power deviation of the operating points detected as the global MPPs by the HCPSO-, PSO- and DE-based methods, from the global MPP derived using the exhaustive-search process, is 0.7%, 32.0%, and 11.1%, respectively, thus indicating the superiority of the proposed HCPSO algorithm to successfully track the global MPP.

As analyzed in Section III, the operation of the proposed HCPSO algorithm is based on the convergence mechanism of the PSO optimization process, but it does not execute random procedures to reinitialize the particles in case of stagnancy. In contrast, the chaotic-search-based initialization of the particles, which is performed in the proposed HCPSO algorithm, distributes them within the search space in a more efficient way, compared to the random initialization performed in the

PSO-based approach. Thus, compared to the PSO algorithm, the HCPSO-based global MPPT method converges to operating points which reside much closer to the global MPP. Also, according to the results presented in Table II, applying the proposed HCPSO method with two particles is the most effective approach in terms of convergence speed, which also outperformed the PSO and DE global MPP methods in case of power–voltage characteristics with either none or one local MPP.

Considering the power–voltage curves of the flexible PV module in Figs. 3 and 4, as well as the experimental results presented in Table II, the performance of the HCPSO, PSO and DE methods, in terms of the power deviation and number of steps, depends on: 1) the operating conditions of the flexible PV module (i.e., bending angle, solar irradiation intensity, etc.), which define the shape of the power–voltage curve, and 2) the randomness inherent in the operation of these global MPPT methods. The performance of the HCPSO and PSO algorithms with two particles and the DE algorithm with four genes, which are the most efficient configurations in terms of convergence speed according to the results presented in Table II, was also experimentally investigated by setting the flexible PV module at various values of θ in the range 0°–180° from 09:00 to 16:00 during two consecutive days. Thus, the impact of direction of the incident solar irradiation on the shape of the power–voltage characteristic of the flexible PV module when installed under bending conditions, as demonstrated in Section II, was also considered in the performance evaluation of the global MPPT methods under study. During the test process, the solar irradiation on horizontal plane and ambient temperature were measured to vary in the range of 320–740 W/m^2 and 18.1–22.7 °C, respectively. The resulting experimentally measured power–voltage characteristics of the flexible PV module are illustrated in Fig. 8(a), showing that test cases are also included where the power–voltage characteristic of the flexible PV module exhibits a local MPP. The average and standard deviation values of the deviation of the PV power produced at the operating point derived by each algorithm as the global MPP, from the power at the global MPP, which was detected by the exhaustive search process, are presented in Fig. 8(b). It is observed that the average power deviation of the proposed HCPSO algorithm from the global MPP detected by the exhaustive-search process is less than the average power deviation of the PSO and DE techniques by 33.9% and 66.1%, respectively. The power deviation of the HCPSO algorithm exhibits a standard deviation, which is lower than that of the PSO and DE algorithms by 41.7% and 55.6%, respectively.

The average and standard deviation values of the number of steps required by each optimization method in order to converge to the global MPP are illustrated in Fig. 8(c). The number of steps required by the HCPSO algorithm in order to accomplish the corresponding global MPPT processes were 20–28 with a standard deviation of 3.53 steps, while the PSO and DE algorithms require a constant number of search steps, since according to the corresponding termination criteria employed, their operation is suspended after a predefined number of iterations. Also, the HCPSO algorithm accomplishes the global MPPT process with 24.8% and 73.2% less average search steps compared to the PSO and DE algorithms, respectively. Thus, using the proposed

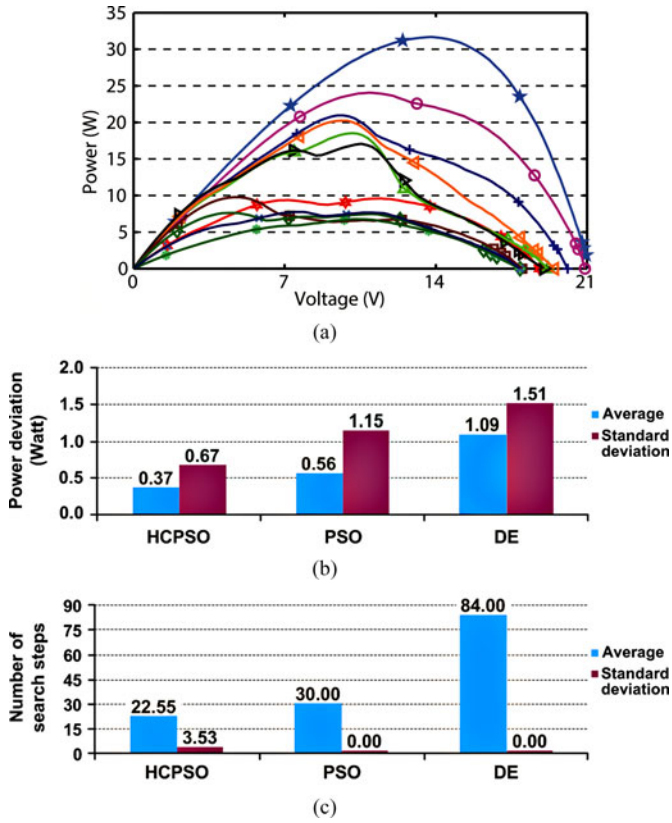

Fig. 8. Performance of the HCPSO, PSO, and DE algorithms: (a) power–voltage characteristics of the flexible PV module during the test process; (b) average and standard deviation of the power deviation from the global MPP; and (c) average and standard deviation of the number of search steps.

HCPSO algorithm the PV power loss during the execution of the global MPPT process is minimized.

In all cases investigated in Table II and Fig. 8, the HCPSO, PSO, DE, and exhaustive-search algorithms have been applied with a 1/128 resolution of the PWM control signal duty cycle. However, the number of steps required by the HCPSO, PSO, and DE algorithms in order to derive the global MPP of the flexible PV module is less than the 128 steps executed by the exhaustive-search algorithm. A common characteristic of the exhaustive-search, HCPSO, PSO, and DE algorithms is that, for a given application, the duty-cycle resolution employed during their execution can be tailored to the dc/dc converter input/output voltage range and the operational characteristics of the flexible PV module, such that the performance of the global MPPT system is optimized in terms of the accuracy of detecting the global MPP and the number of steps required until convergence.

In order to demonstrate the evolution of the global MPPT process, which is performed using the proposed HCPSO method in case that local MPPs are exhibited by the power–voltage characteristic of the PV module, the experimentally measured power–voltage characteristic of the flexible PV module in case that $\theta = 180^\circ$ and $\beta = \alpha = 0^\circ$ at 13:00 of a clear-sky winter day is shown in Fig. 9(a). The output power of the flexible PV module at each step of operation of the HCPSO algorithm with three particles is also depicted in that figure. The experimentally measured trajectory of consecutive flexible PV module output

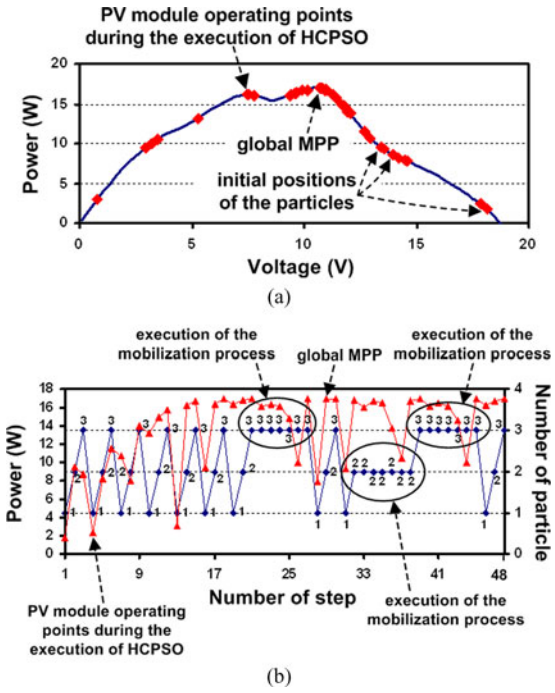

Fig. 9. Experimental results of the HCPSO algorithm with three particles in case that $\theta = 180°, \beta = \alpha = 0°$, the incident solar irradiation is equal to 730 W/m^2 and the ambient temperature is 22.7 °C at 13:00 of a clear-sky winter day: (a) the power–voltage characteristic of the flexible PV module and the operating points during the operation of the HCPSO algorithm and (b) the flexible PV module output power at each search step of the HCPSO algorithm for each particle.

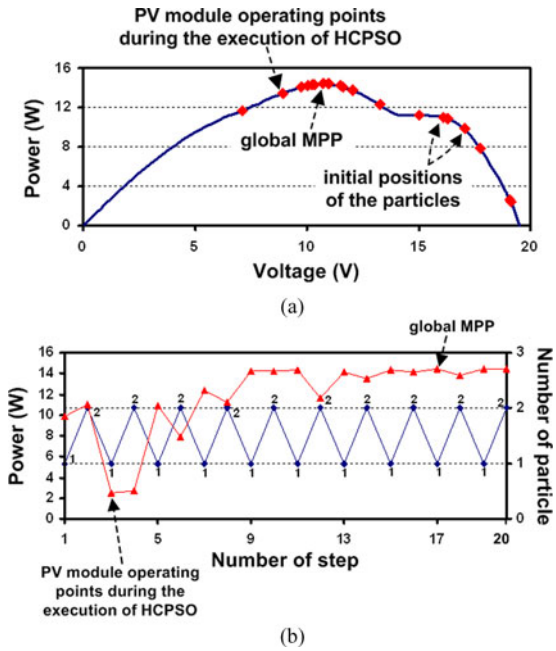

Fig. 10. Experimental results of the HCPSO algorithm with two particles in case that $\theta = 180°, \beta = \alpha = 0°$, the incident solar irradiation is equal to 440 W/m^2 and the ambient temperature is 26.5 °C at 17:00 of a clear-sky summer day: (a) the power–voltage characteristic of the flexible PV module and the operating points during the operation of the HCPSO algorithm and (b) the flexible PV module output power at each search step of the HCPSO algorithm for each particle.

power levels followed by each of the three particles during the operation of the HCPSO algorithm is illustrated in Fig. 9(b). As indicated in Fig. 9(b), the global MPPT process is accomplished in 48 search steps and the chaotic-search-based mobilization mechanism of the HCPSO algorithm (see Fig. 6) is activated during time steps 21–27, 32–38, and 39–45, respectively. It is observed that the three particles of the HCPSO algorithm started exploring the power–voltage search space from a completely different position with respect to the area where the global MPP resides. However, they progressively moved toward the correct direction by successfully discriminating the local and global MPPs, although their power levels do not differ significantly. The position of the global MPP was detected by the second particle at step 29 with a power deviation of 0.55%.

Similarly, the experimentally measured power–voltage characteristic of the flexible PV module in case that $\theta = 180°$ and $\beta = \alpha = 0°$ at 17:00 of a clear-sky summer day, as well as the output power of the flexible PV module during the evolution of the proposed HCPSO algorithm with two particles, are presented in Fig. 10(a). The experimentally measured trajectory, which was followed by the two particles during the HCPSO global MPPT process are shown in Fig. 10(b). In this test case, it was not required for the mobilization mechanism of the HCPSO algorithm (see Fig. 6) to be activated during the execution time steps. Also, the initial positions of the HCPSO algorithm particles were close to the area of a local MPP, which extended over a relatively wide voltage range, but both particles avoided to get trapped in that area. Thus, the global MPP was detected by the first particle at step 17 with a power deviation of 0.22%, while the HCPSO algorithm terminated after executing 20 search steps.

The experimental results indicate that using the same values of the operational parameters, which were derived during the initial test process, the proposed global MPPT system was capable to operate effectively over a wide range of solar irradiation conditions and bending-angle setups, without requirement to repeat the initial parameters-detection process. Each of these operating conditions resulted in different forms of the flexible PV module power–voltage curves, which were not known a priori. However, the proposed HCPSO algorithm was capable to successfully adapt to these different operational characteristics of the flexible PV module power source, which are typically determined by the target application of the PV system, without requiring any knowledge of them.

V. Conclusion

The use of flexible PV modules has emerged during the past few years due to their capability to easily adapt on nonplanar surfaces. However, when installed on curved surfaces the power–voltage characteristic of the flexible PV modules exhibits local MPPs. The experimental results presented in this paper, for the first time in the existing literature, demonstrate that the number and position of local MPPs depends on the solar irradiation and ambient temperature conditions, as well as the installation geometry of the flexible PV module.

A new method of tracking the global MPP of flexible PV modules has also been proposed in this paper, which, compared to the past-proposed MPPT techniques, has the advantage that it is capable to detect the global MPP of flexible PV modules with less search steps. The performance superiority of the proposed global MPPT technique over the past-proposed methods has been demonstrated with a comparative experimental study under real operating conditions. Applying the proposed HCPSO method with two particles was the most effective approach in terms of convergence speed. Thus, using the proposed system, the power loss during the global MPPT process is minimized and the energy production of the flexible PV module is maximized.

The boost-converter-based design, which has been presented in the paper, is directly applicable to distributed MPPT architectures of PV systems comprising flexible PV modules [34]. Also, the microcontroller-based control unit can be easily modified to control, according to the proposed HCPSO algorithm, alternative dc/dc power converter topologies (e.g., buck, buck–boost, etc.) in order to adapt to specific operational requirements of the target PV application.

REFERENCES

[1] F. Boico and B. Lehman, "Multiple-input maximum power point tracking algorithm for solar panels with reduced sensing circuitry for portable applications," *Solar Energy*, vol. 86, pp. 463–475, 2012.

[2] A. W. Blakers and T. Armour, "Flexible silicon solar cells," *Solar Energy Mater. Solar Cells*, vol. 93, pp. 1440–1443, 2009.

[3] K. M. Trautz, P. P. Jenkins, R. J. Walters, D. Scheiman, R. Hoheisel, R. Tatavarti, R. Chan, H. Miyamoto, J. G. J. Adams, V. C. Elarde, and J. Grimsley, "Mobile solar power," *IEEE J. Photovoltaics*, vol. 3, no. 1, pp. 535–541, Jan. 2013.

[4] K. M. Edmondson, D. C. Law, G. Glenn, A. Paredes, R. R. King, and N. H. Karam, "Flexible III–V multijunction solar blanket," in *Proc. IEEE 4th World Conf. Photovoltaic Energy Convers.*, vol. 2, 2006, pp. 1935–1938.

[5] E. Thomsen, J. Muric-Nesic, V. Everett, M. Brauers, E. Davies, T. Ratcliff, C. Samundsett, I. Skryabin, L. Xia, and A. Blakers, "Materials and manufacturing processes for high-efficiency flexible photovoltaic modules," in *Proc. 35th IEEE Photovoltaic Spec. Conf. (PVSC)*, 2010, pp. 2877–2882.

[6] E. A. Thomsen, J. Muric-Nesic, S. Rahman, Y. O. Mayon, D. Wang, T. Ratcliff, V. Everett, I. Skryabin, and A. Blakers, "Flexible sliver modules," *37th IEEE Photovoltaic Spec. Conf. (PVSC)*, pp. 3225–3230, 2011.

[7] P. Reinhard, A. Chirilă, P. Blösch, F. Pianezzi, S. Nishiwaki, S. Buecheler, and A. N. Tiwari, "Review of progress toward 20% efficiency flexible CIGS solar cells and manufacturing issues of solar modules," *IEEE J. Photovoltaics*, vol. 3, no. 1, pp. 572–580, Jan. 2013.

[8] C. R. Sullivan, J. J. Awerbuch, and A. M. Latham, "Decrease in photovoltaic power output from ripple: Simple general calculation and the effect of partial shading," *IEEE Trans. Power Electron.*, vol. 28, no. 2, pp. 740–747, Feb. 2013.

[9] L. V. Hartmann, M. A. Vitorino, M. B. R. Correa, and A. M. N. Lima, "Combining model-based and heuristic techniques for fast tracking the maximum power point of photovoltaic systems," *IEEE Trans. Power Electron.*, vol. 28, no. 6, pp. 2875–2885, Jun. 2013.

[10] E. Dallago, D. G. Finarelli, U. P. Gianazza, A. L. Barnabei, and A. Liberale, "Theoretical and experimental analysis of an MPP detection algorithm employing a single-voltage sensor only and a noisy signal," *IEEE Trans. Power Electron.*, vol. 28, no. 11, pp. 5088–5097, Nov. 2013.

[11] G.-C. Hsieh, H.-I Hsieh, C.-Y. Tsai, and C.-H. Wang, "Photovoltaic power-increment-aided incremental-conductance MPPT with two-phased tracking," *IEEE Trans. Power Electron.*, vol. 28, no. 6, pp. 2895–2911, Jun. 2013.

[12] Y. Jiang, J. A. A. Qahouq, and T. A. Haskew, "Adaptive step size with adaptive-perturbation-frequency digital MPPT controller for a single-sensor photovoltaic solar system," *IEEE Trans. Power Electron.*, vol. 28, no. 7, pp. 3195–3205, Jul. 2013.

[13] A. K. Abdelsalam, A. M. Massoud, S. Ahmed, and P. Enjeti, "High-performance adaptive perturb and observe MPPT technique for photovoltaic-based microgrids," *IEEE Trans. Power Electron.*, vol. 26, no. 4, pp. 1010–1021, Apr. 2011.

[14] A. M. Latham, R. Pilawa-Podgurski, K. M. Odame, and C. R. Sullivan, "Analysis and optimization of maximum power point tracking algorithms in the presence of noise," *IEEE Trans. Power Electron.*, vol. 28, no. 7, pp. 3479–3494, Jul. 2013.

[15] B. Subudhi and R. Pradhan, "A comparative study on maximum power point tracking techniques for photovoltaic power systems," *IEEE Trans. Sustainable Energy*, vol. 4, no. 1, pp. 89–98, Jan. 2013.

[16] D. C. Jones and R. W. Erickson, "Probabilistic analysis of a generalized perturb and observe algorithm featuring robust operation in the presence of power curve traps," *IEEE Trans. Power Electron.*, vol. 28, no. 6, pp. 2912–2926, Jun. 2013.

[17] P. S. Shenoy, K. A. Kim, B. B. Johnson, and P. T. Krein, "Differential power processing for increased energy production and reliability of photovoltaic systems," *IEEE Trans. Power Electron.*, vol. 28, no. 6, pp. 2968–2979, Jun. 2013.

[18] R. C. N. Pilawa-Podgurski and D. J. Perreault, "Sub-module integrated distributed maximum power point tracking for solar photovoltaic applications," *IEEE Trans. Power Electron.*, vol. 28, no. 6, pp. 2957–2967, Jun. 2013.

[19] S. M. MacAlpine, R. W. Erickson, and M. J. Brandemuehl, "Characterization of power optimizer potential to increase energy capture in photovoltaic systems operating under nonuniform conditions," *IEEE Trans. Power Electron.*, vol. 28, no. 6, pp. 2936–2945, Jun. 2013.

[20] L. F. L. Villa, T.-P. Ho, J.-C. Crebier, and B. Raison, "A power electronics equalizer application for partially shaded photovoltaic modules," *IEEE Trans. Ind. Electron.*, vol. 60, no. 3, pp. 1179–1190, Mar. 2013.

[21] I. Abdalla, J. Corda, and L. Zhang, "Multilevel DC-link inverter and control algorithm to overcome the PV partial shading," *IEEE Trans. Power Electron.*, vol. 28, no. 1, pp. 14–18, Jan. 2013.

[22] Y.-H. Ji, D.-Y. Jung, J.-G. Kim, J.-H. Kim, T.-W. Lee, and C.-Y. Won, "A real maximum power point tracking method for mismatching compensation in PV array under partially shaded conditions," *IEEE Trans. Power Electron.*, vol. 26, no. 4, pp. 1001–1009, Apr. 2011.

[23] B. N. Alajmi, K. H. Ahmed, S. J. Finney, and B. W. Williams, "A maximum power point tracking technique for partially shaded photovoltaic systems in microgrids," *IEEE Trans. Ind. Electron.*, vol. 60, no. 4, pp. 1596–1606, Apr. 2013.

[24] P. K. Peter and V. Agarwal, "On the input resistance of a reconfigurable switched capacitor DC–DC converter-based maximum power point tracker of a photovoltaic source," *IEEE Trans. Power Electron.*, vol. 27, no. 12, pp. 4880–4893, Dec. 2012.

[25] A. Bidram, A. Davoudi, and R. S. Balog, "Control and circuit techniques to mitigate partial shading effects in photovoltaic arrays," *IEEE J. Photovoltaics*, vol. 2, no. 4, pp. 532–546, Oct. 2012.

[26] J. P. Storey, P. R. Wilson, and D. Bagnall, "Improved optimization strategy for irradiance equalization in dynamic photovoltaic arrays," *IEEE Trans. Power Electron.*, vol. 28, no. 6, pp. 2946–2956, Jun. 2013.

[27] S. Syafaruddin, T. Hiyama, and E. Karatepe, "Investigation of ANN performance for tracking the optimum points of PV module under partially shaded conditions," in *Proc. Conf. Proc. IPEC*, 2010, pp. 1186–1191.

[28] T. L. Nguyen and K.-S. Low, "A global maximum power point tracking scheme employing DIRECT search algorithm for photovoltaic systems," *IEEE Trans. Ind. Electron.*, vol. 57, no. 10, pp. 3456–3467, Oct. 2010.

[29] L. Zhou, Y. Chen, K. Guo, and F. Jia, "New approach for MPPT control of photovoltaic system with mutative-scale dual-carrier chaotic search," *IEEE Trans. Power Electron.*, vol. 26, no. 4, pp. 1038–1048, Apr. 2011.

[30] K. Ishaque, Z. Salam, M. Amjad, and S. Mekhilef, "An improved particle swarm optimization (PSO)-based MPPT for PV with reduced steady-state oscillation," *IEEE Trans. Power Electron.*, vol. 27, no. 8, pp. 3627–3638, Aug. 2012.

[31] M. Miyatake, M. Veerachary, F. Toriumi, N. Fujii, and H. Ko, "Maximum power point tracking of multiple photovoltaic arrays: A PSO approach," *IEEE Trans. Aerosp. Electron. Syst.*, vol. 47, no. 1, pp. 367–380, Jan. 2011.

[32] H. Taheri, Z. Salam, K. Ishaque, and S. Syafaruddin, "A novel maximum power point tracking control of photovoltaic system under partial and rapidly fluctuating shadow conditions using differential evolution," in *Proc. IEEE Symp. Ind. Electron. Appl. (ISIEA)*, 2010, pp. 82–87.

[33] K. Ishaque and Z. Salam, "A deterministic particle swarm optimization maximum power point tracker for photovoltaic system under partial shading condition," *IEEE Trans. Ind. Electron.*, vol. 60, no. 8, pp. 3195–3206, Aug. 2013.

[34] M. Acanski, J. Popovic-Gerber, and J. A. Ferreira, "Thermal modeling of the module integrated DC–DC converter for flexible thin-film PV modules," in *Proc. 14th Eur. Conf. Power Electron. Appl. (EPE)*, 2011, pp. 1–10.
[35] P. Sharma, B. Patnaik, S. P. Duttagupta, and V. Agarwal, "Dynamic power optimization of contoured flexible PV array under non-uniform illumination conditions," in *Proc. 35th IEEE Photovoltaic Spec. Conf. (PVSC)*, 2010, pp. 968–972.
[36] N. Mohan, T. M. Undeland, and W. P. Robbins, *Power Electronics: Converters, Applications, and Design*, 2nd ed. New York, NY, USA: Wiley, 1995.
[37] J. G. Kassakian, M. F. Schlecht, and G. C. Verghese, *Principles Power Electron.*, 2nd ed. Reading, MA, USA: Addison-Wesley, 1992.
[38] H. Meng, P. Zheng, R. Wu, X. Hao, and Z. Xie, "A hybrid particle swarm algorithm with embedded chaotic search," in *Proc. IEEE Conf. Cybern. Intell. Syst.*, 2004, vol. 1, pp. 367–371.

Christos Konstantopoulos was born in Athens, Greece, in 1989. He received the B.Sc. degree in 2012 from the Department of Electronic and Computer Engineering, Technical University of Crete, Chania, Greece, where he is currently working toward the M.Sc. degree.

His current research interests include power electronics for renewable energy sources, energy harvesting for wireless sensor networks, and electronic measurement systems.

Eftichios Koutroulis (M'10) was born in Chania, Greece, in 1973. He received the B.Sc., M.Sc., Ph.D. [in the area of power electronics and renewable energy sources (RES)] degrees from the Department of Electronic and Computer Engineering, Technical University of Crete, Chania, Greece, in 1996, 1999, and 2002, respectively.

He is currently an Assistant Professor in the Department of Electronic and Computer Engineering, Technical University of Crete. His current research interests include power electronics (dc/ac inverters, dc/dc converters), the development of microelectronic energy management systems for RES, and the design of photovoltaic and wind energy conversion systems.